scientific reports

Check for updates

OPEN

The value of nomogram analysis in predicting pulmonary metastasis in hepatic alveolar echinococcosis

Changyou Long[1,2], Yeang Danzeng[1,2], Pengqi Tian[1], Yujie Xing[1], Xueqian Zhang[1] & Haihua Bao[1]✉

Hepatic alveolar echinococcosis (HAE) is a rare zoonotic parasitic disease that closely resembles malignant tumors in both behavior and appearance. It can cause infiltration of affected organs and chronic liver damage. In advanced stages, it may metastasize or invade surrounding organs, resembling liver cancer, and is clinically referred to as "parasitic cancer." However, the prognosis of HAE with pulmonary metastasis is poor, and no reliable method currently exists to predict lung metastasis. This study aims to investigate the efficacy of a nomogram model, based on CT and MRI imaging features in conjunction with clinical indicators, for predicting pulmonary metastasis in HAE. A retrospective analysis was conducted using imaging and clinical data from 297 patients diagnosed with HAE. Univariate and multivariate logistic regression analyses identified independent factors associated with pulmonary metastasis, including lesion size, the presence of metastasis to other organs, cavitary lesions, and enhancement characteristics. The nomogram, developed using these variables, demonstrated strong predictive performance in both the training and validation cohorts. This model provides an effective tool for predicting the risk of pulmonary metastasis, offering early insights into disease progression and assisting clinicians in formulating personalized treatment and prognostic plans.

Keywords Hepatic alveolar echinococcosis, Pulmonary metastasis, Nomogram, Magnetic resonance imaging, Computed tomography imaging, Parasites

Echinococcosis can currently be classified into cystic echinococcosis, alveolar echinococcosis (AE), E. granulosus sensu lato, and neotropical echinococcosis[1]. Among them, cystic echinococcosis and AE caused by Echinococcus granulosus and Echinococcus multilocularis pose a particularly significant threat to public health[2]. Both of these diseases are serious and critically urgent. Especially AE, without proper or timely treatment, has a high fatality rate and poor prognosis[3–5]. This imposes a heavy health burden on patients and causes significant economic losses. Therefore, it is also considered one of the most dangerous human parasitic diseases[6,7].

AE is a rare zoonotic parasitic disease[8], with foxes and dogs as the definitive hosts and rodents as the main intermediate hosts. Although humans, cattle, sheep, and other animals are not the most suitable intermediate hosts for Echinococcus multilocularis, they may still become infected and develop the disease through opportunistic infections. In 98% of cases, the liver is the primary target organ involved in AE[9], and due to its exogenous budding or infiltrative proliferation, it continuously produces new vesicles that grow into tissues, behaving and appearing similar to malignant tumors. This can cause infiltration of the affected organs and chronic damage to liver tissue. In late stages, metastasis or invasion of surrounding organs is similar to liver cancer, earning it the clinical nickname of "parasitic cancer."

Hepatic alveolar echinococcosis (HAE) can metastasize to the pulmonary organs, brain, spleen, kidneys, heart, bones, and other organs in the middle and late stages, with the pulmonary organs often being the first and most common site[10]. When HAE metastasizes to the pulmonary system, the clinical prognosis for patients is often poor, making early diagnosis extremely important. According to the recommendations of the World Health Organization-Informal Working Group on Echinococcosis (WHO-IWGE) expert consensus[11], radical surgical resection is the preferred treatment for early-stage patients with entirely resectable lesions. However, for patients who are not candidates for surgical treatment (such as those with pulmonary metastasis), long-term anti-infective therapy with mebendazole or the now more commonly used albendazole (both benzimidazole

[1] Imaging Center, Qinghai University Affiliated Hospital, Xining 810001, China. [2]Changyou Long and Yeang Danzeng contributed equally to this work. ✉email: baohelen2@sina.com

compounds) can be administered. Thus, predicting whether HAE will progress to pulmonary metastasis holds significant clinical value.

Previous studies on prediction models have primarily focused on using omics technologies to predict the biological activity[12], brain metastasis[13], and lymph node metastasis of HAE[14]. In addition, some studies have assessed the biological activity of the lesions themselves and their surrounding tissues through nomogram models[15]. Other studies have conducted prognostic prediction analyses for end-stage patients undergoing liver resection or autologous liver transplantation[16]. These studies have provided important theoretical and technical support for the diagnosis and treatment of HAE. This study is specifically focused on the prediction of pulmonary metastasis in HAE. A nomogram prediction model based on HAE imaging characteristics and clinical indicators has been constructed, enabling the quantitative and intuitive analysis of the probability of pulmonary metastasis in patients. This model helps in the early, accurate, convenient, and non-invasive identification of potential risk factors for pulmonary metastasis, providing a basis for selecting individualized treatment plans for HAE patients.

Materials and methods

General information

This study was approved by the Ethics Committee of the Clinical Medical College of Qinghai University (Approval No: P-SL-2023-229). Due to the retrospective nature of the study, the requirement for informed consent was waived by the Ethics Committee of the Clinical Medical College of Qinghai University. The study protocol followed the principles of the Declaration of Helsinki, and all procedures complied with the national and institutional ethical standards.

Retrospectively collected imaging features and clinical indicators of patients first diagnosed with HAE at the Qinghai University Affiliated Hospital from 2015 to 2022. Inclusion criteria: (1) Pathologically confirmed as HAE after surgery or meeting the diagnostic criteria in the "Expert Consensus on Imaging Diagnosis of Hepatic Echinococcosis"[17]; (2) Complete clinical data of the patients; (3) All patients underwent dynamic contrast-enhanced CT scanning of the abdominal cavity in three phases and chest CT examination. Exclusion criteria: (1) Presence of other tumorous diseases in the liver. (2) Inability to evaluate due to severe image artifacts, as shown in Fig. 1. Two hundred ninety-seven patients with hepatic alveolar echinococcosis were included, comprising 138 males and 159 females, with an average age of 39.23 ± 14.03 years. Using the "Random Number Generator" in SPSS software, patients were randomly allocated to the training set and test set in a 7:3 ratio. Subsequently, the training set data was used for model construction, and the test set data was used to verify the model's effectiveness.

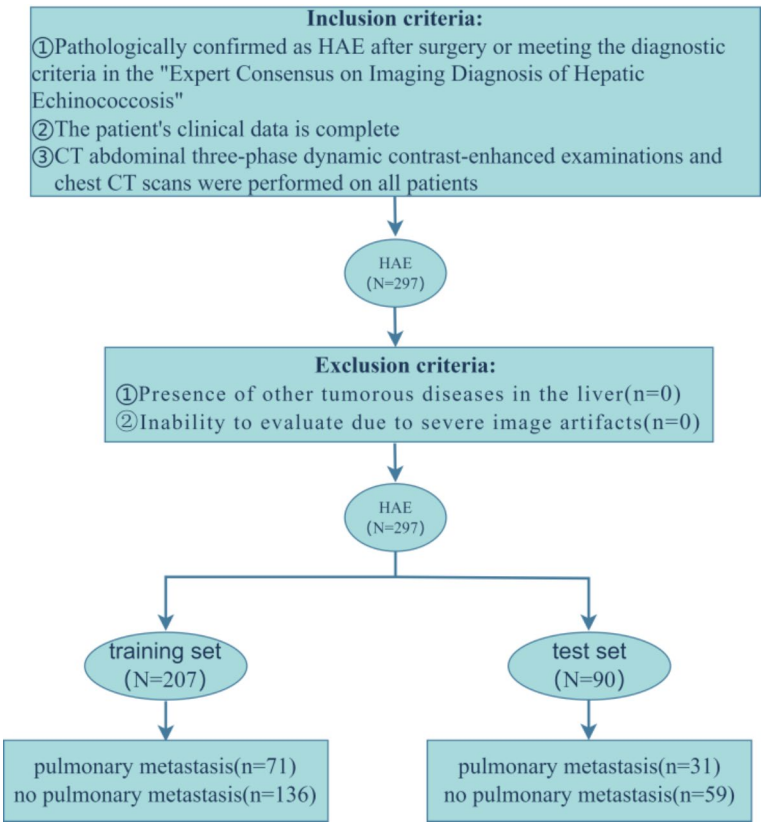

Fig. 1. Flowchart of patient inclusion and exclusion criteria. HAE = hepatic alveolar echinococcosis.

Examination methods

CT examination

All patients underwent abdominal three-phase dynamic contrast-enhanced CT scanning and chest CT plain scan with enhancement using a 128-slice spiral CT scanner (Discovery CT 750 HD; GE Medical Systems, Milwaukee, Wis). The abdominal scanning range extended from the rib cage to the iliac bones, with patients lying supine. The scanning parameters were as follows: tube voltage of 80-120KV, tube current of 200 mA, slice thickness of 5 mm, and rotation time of 0.5 s per revolution. First, a plain scan was performed, followed by a contrast-enhanced scan. The contrast agent used was ioversol injection (350 mg L/ml), administered through the median cubital vein at a 4–5 ml/s rate. Threshold tracking was employed for scanning, and once the threshold of 120HU was reached, the scan was automatically triggered. With a minimum delay of 2 s after reaching the threshold, the first phase (aortic phase) was scanned. Subsequently, after a delay of 25 s, the second phase (portal venous phase) was scanned, followed by a delay of 40 s for the third phase (delayed phase) scan. The scanning range for the chest encompassed the thoracic inlet to the base of the pulmonary region, with the patient positioned in a supine layout. The scanning parameters were set as follows: a tube voltage of 120 KV, a tube current of 10 mA, a slice thickness of 1.25 mm, and a rotation time of 0.5 s per revolution. First, a plain scan was performed, followed by a contrast-enhanced scan. The contrast agent used was ioversol injection (350 mg L/ml), administered through the median cubital vein at a rate of 2.0-2.6 ml/s.

MRI examination

Fifty patients did not undergo MRI examination for special reasons, while the remaining 247 underwent abdominal MRI plain scan, DWI, and contrast-enhanced scan. MRI data was acquired using Siemens Prisma 3.0T and Philips Archieva 3.0T magnetic resonance scanners with abdominal coils. The scanning sequences included: (1) Axial in-phase and out-of-phase T1WI: TR 5.16ms, TE 1.35ms, slice thickness 4.0 mm, FOV 284.4 mm, matrix 195 × 320. (2) Axial T2WI: TR 3600ms, TE 76ms, slice thickness 6 mm, FOV 284.4 mm, matrix 182 × 320. (3) Axial contrast-enhanced T1WI: TR 5.19ms, TE 1.35ms, slice thickness 4.0 mm, FOV 284.4 mm, matrix 182 × 320. (4) DWI sequence: TR 7000ms, TE 58ms, slice thickness 6 mm, FOV 308.8 mm, matrix 104 × 128. First, a plain scan was performed, followed by a contrast-enhanced scan. The contrast agent used was gadoxetic acid disodium injection, administered through the median cubital vein at a dose of 0.1 ml/kg body weight over 12 s, followed by a flush of 20 ml of saline. Arterial phase, portal venous phase, and equilibrium phase images were acquired with delays of 20 s, 60 s, and 3 min, respectively.

Criteria for assessing pulmonary metastasis and definitions of other imaging signs

Pulmonary metastasis is deemed to have occurred if the following two criteria are met: (1) Pathological confirmation of pulmonary lesions following surgery. (2) A comprehensive assessment based on the following criteria: (a) Presence of a definite primary pulmonary lesion of HAE, as illustrated in Fig. 2; (b) Positive immunological test results for HAE, such as Enzyme-Linked Immunosorbent Assay (ELISA); (c) Pulmonary lesions exhibiting typical CT findings (e.g., multiple soft tissue density nodules of varying sizes in the peripheral zones of both lungs, often accompanied by cavitation and calcification), consistent with the imaging manifestations described by Eroglu et al.[18], as depicted in Fig. 3.

Calcification signs: Punctate calcified particles can be seen within the lesion, accompanied by flocculent or irregularly large calcified foci. Cavity signs: The larvae proliferate into large lesions, with internal coagulation and vascular occlusion, which further lead to localized ischemic necrosis and liquefaction into irregular gelatinous substances, sometimes presenting crab claw-like liquefied cavities[19]. Marginal zone: The lesion has an unclear margin, showing infiltrative growth, rich in neovascularization and inflammatory cells; DWI shows a high signal area, and dynamic enhancement shows mild enhancement. Microvesicles: Small honeycomb or cystic structures are present within and at the edge of the lesion, showing high signal intensity on both T2WI and MRCP. Bile duct invasion: Hepatic bile ducts are infiltrated by lesions or have unclear boundaries with lesions, dilation, or bile duct obstruction[20]. Vascular invasion: Defined as morphologically recognizable vascular lumen infiltration, no contrast agent filling after vascular occlusion, or associated thrombosis[21].

Image analysis and clinical data

Two radiologists with ten years of diagnostic experience independently analyzed the abdominal and chest CT scans. In the event of any disagreement between the two radiologists regarding the interpretation of pulmonary metastasis on the chest CT, a chief physician with over 30 years of experience in imaging diagnosis made the final determination. The collected imaging features encompass the number, size, and type of lesions, PNM stages, extent of hepatic involvement, as well as the presence or absence of calcification signs, cavity signs, enhancement, marginal zone, microvesicles, bile duct dilation, bile duct invasion, hepatic gate invasion, hepatic vein invasion, inferior vena cava invasion, hepatic artery invasion, portal vein invasion, and other organ metastases. In multiple lesions, the lesion size refers to the maximum diameter of the most significant lesion. The intraclass correlation coefficient(ICC) was used to evaluate the consistency of measurements between the two doctors. An ICC greater than 0.75 indicated good consistency, and the average measurement value of the two doctors was then taken for further analysis. In addition, the clinical characteristics of the patients were collected, including sex, age, ethnic group, exposure history to cattle and sheep, HBV five markers, treatment methods, and complications.

Establishment and evaluation of prediction models

In this study, a nomogram model was constructed using the training dataset. Univariate and multivariate logistic regression analyses were employed to screen imaging and clinical indicators for predicting HAE pulmonary metastasis, and the resulting independent predictors were used to build the nomogram model. The model's predictive ability was evaluated using the receiver operating characteristic (ROC) curve, and the area under the

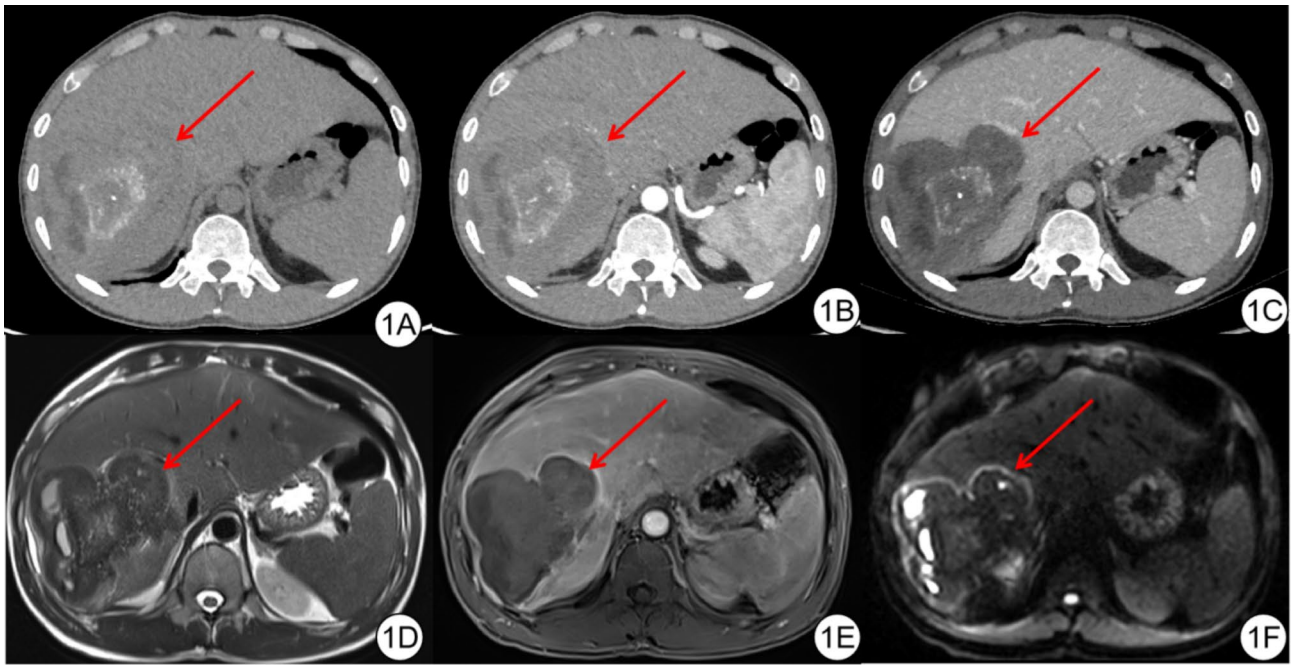

Fig. 2. Imaging manifestations of HAE, (**A**): the non-contrast CT scan shows a lesion in the liver's S6 segment with mixed density and unclear borders. (**B**): During the arterial phase of contrast-enhanced CT, the lesion in liver segment S6 appears non-enhancing, with mild enhancement of the surrounding liver parenchyma, resulting in better delineation of the lesion borders. (**C**) During the venous phase of contrast-enhanced CT, the lesion in liver segment S6 shows no significant enhancement, while there is marked enhancement of the surrounding liver parenchyma, leading to a clear delineation of the lesion borders. (**D**) T2WI shows a liver lesion in segment 6 with a mixed high and low signal intensity, with clear borders. (**E**): Contrast-enhanced T1WI shows no noticeable enhancement in the liver lesion of segment 6, with an enhanced rim at the edge. (**F**): DWI shows a liver lesion in segment 6 with mixed high and low signal intensity and a rim of high signal intensity at the edge.

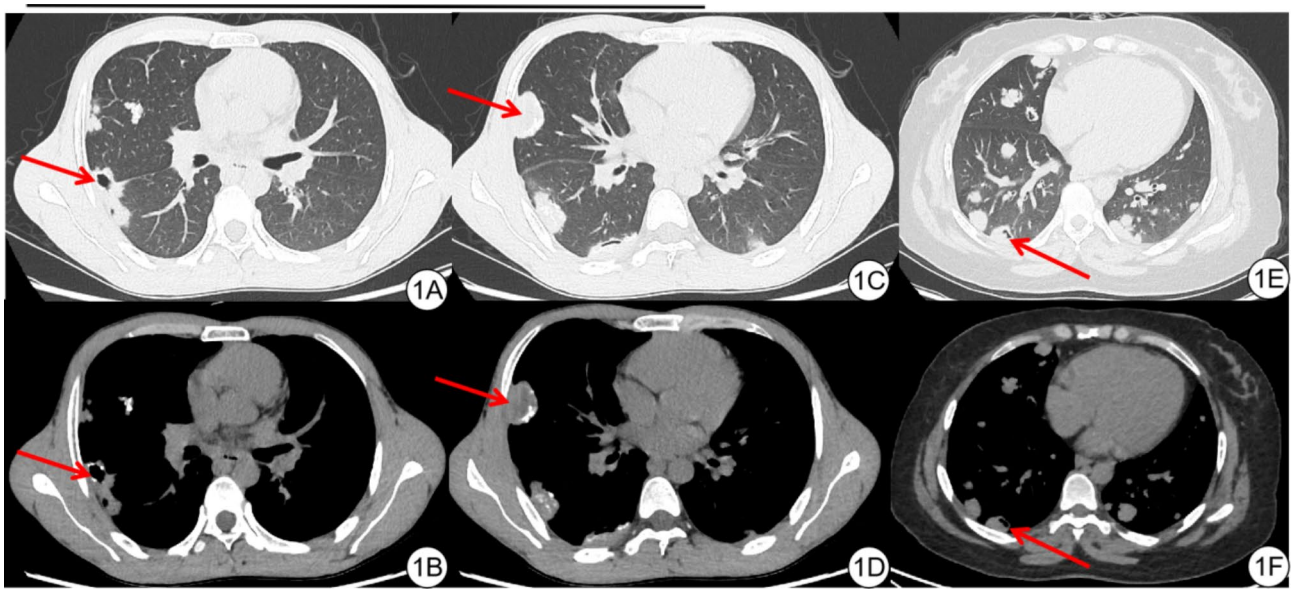

Fig. 3. Imaging Manifestations of pulmonary metastases in HAE, (**A**–**F**): The lung and soft tissue windows show multiple nodular soft tissue density lesions with varying sizes located outside both lungs, with some showing calcifications and cavitation features.

curve (AUC), as well as sensitivity and specificity, were calculated based on the maximum value of the Youden index. Simultaneously, calibration curves (CRC) were employed to evaluate the model's goodness of fit, ensuring its stable and reliable performance in the test set. In addition, to more comprehensively evaluate the clinical value of the prediction model, we introduced decision curve analysis (DCA) to quantify the net benefit to patients across different threshold probabilities. This approach was used to assess the clinical utility of the prediction model and select the optimal model.

Statistical analysis

Statistical analysis was performed using RStudio 4.3.2, Medcalc 20.022, and SPSS 25. In SPSS 25, the Shapiro-Wilk test was first used to check the normality of continuously distributed data. Those conforming to the normal distribution were expressed as Mean ± SDs, and independent sample t-tests were used to compare the two groups. Categorical variables are expressed in frequencies, and comparisons between the two groups are made using the chi-square test. Univariate analysis was performed using independent sample t-tests or chi-square tests, and influencing factors with $p < 0.05$ were selected for inclusion in multivariate logistic regression analysis. ROC curves were drawn using Medcalc. The nomogram and calibration curves were plotted using the rms package in R, while decision curves were created with the rmda package. A p-value of less than 0.05 was considered statistically significant.

Results

Clinical data

Among 297 patients with HAE, 207 cases were included in the training set (38 of whom underwent only CT examination, while the remainder underwent CT and MRI examination). These comprised 96 males and 111 females, with a mean age of 38.84 ± 13.93 years. Within this group, 136 cases did not experience pulmonary metastasis, while 71 did. The test set included 90 cases (14 of whom underwent only CT examination, while the remainder underwent both CT and MRI examination), consisting of 42 males and 48 females, with a mean age of 40.13 ± 14.29 years. Among these, 59 cases did not have pulmonary metastasis, while 31 did. There were no statistically significant differences in imaging and clinical indicators between the training and test sets ($p > 0.05$). Details are shown in Table 1.

Evaluation of consistency among feature groups

Consistency was assessed using the ICC. The ICC values for the imaging features extracted by two radiologists ranged from 0.83 to 0.98. Since ICC > 0.75 indicates good consistency, the average measurements from the two radiologists were taken for further analysis.

Development of prediction models and nomograms

The model was constructed using the training set data. Firstly, a univariate analysis was performed on the training set. It was found that there were statistically significant differences in age, size, extent of hepatic involvement, treatment methods, cavity signs, as well as whether there was enhancement, hepatic gate invasion, bile duct dilation, exposure history to cattle and sheep, and other organ metastases (all $p < 0.05$). Details are shown in Table 2. After incorporating these factors into multivariate Logistic regression analysis, it was found that lesion size, other organ metastases, cavity signs, and enhancement were independent predictors of pulmonary metastasis in patients with HAE (all with $p < 0.05$). Details are provided in Fig. 4. Based on these four independent predictors, a prediction model for pulmonary metastasis in HAE was constructed, and a nomogram was drawn using the R language. In the nomogram, the green lines represent the 95% confidence intervals for each predictor. Please refer to Fig. 5 for details.

Effectiveness and validation of the nomogram prediction model

In the training set, the AUC value for predicting pulmonary metastasis in HAE was maximized at a cutoff value of 0.5498, resulting in an AUC of 0.841 (95% CI: 0.785–0.897), with a sensitivity of 70.42% and a specificity of 84.56%. In the test set, the AUC value for predicting pulmonary metastasis in HAE was maximized at a cutoff value of 0.6490, resulting in an AUC of 0.835 (95% CI: 0.745–0.924), with a sensitivity of 90.32% and a specificity of 74.58%. Please refer to Fig. 6 for details. The prediction performance of the model was validated using CRC. The CRC for the training set showed a mean absolute error of 0.036, while the CRC for the test set showed a mean absolute error of 0.042. This indicates good agreement between the model's predictions and actual clinical outcomes. Please refer to Fig. 7 for details. The clinical application value of the model was validated through DCA. The results showed that using the model to predict pulmonary metastasis in HAE would yield more excellent clinical benefits within a specific range, demonstrating that this prediction model has significant clinical application value. Please refer to Fig. 8 for details.

Discussion

AE has a long incubation period, low incidence rate, diagnostic difficulties, malignant tumor growth characteristics, and poor clinical prognosis after metastasis. Without timely treatment, 90% of patients will die within 10–15 years after infection[9]. Treatment choice frequently varies depending on the presence or absence of metastasis[11,22,23], with the pulmonary system often being the first and most common site of metastasis in AE. Therefore, identifying the factors that predict pulmonary metastasis in HAE is crucial for selecting appropriate treatment options and predicting clinical prognosis for patients. Through in-depth analysis of clinical indicators, CT, and MRI imaging signs of HAE, this study found that lesion size, other organ metastases, cavity signs, and enhancement are independent predictors of pulmonary metastasis in HAE. The nomogram model constructed

Factors	Training (207)	Test (90)	Statistical values	*p*-values
Sex/case (%)			0.002[a]	0.963
Male	96(46.4)	42(46.7)		
Female	111(53.6)	48(53.3)		
Age/Y	38.84 ± 13.93	40.13 ± 14.29	0.732[b]	0.465
Ethnic group/case (%)			1.453[a]	0.228
Tibet	181(87.4)	83(92.2)		
Other	26(12.6)	7(7.8)		
Marginal zone /case (%)*			2.886[a]	0.089
No	39(46.4)	10(29.4)		
Yes	45(53.6)	24(70.6)		
Microvesicles/case (%)*			1.138[a]	0.286
No	51(60.7)	17(50.0)		
Yes	33(39.3)	17(50.0)		
Number of lesions/case (%)			0.617[a]	0.432
One	143(69.1)	58(64.4)		
Two or more	64(30.9)	32(35.6)		
Lesion size/case (%)			0.809[a]	0.667
≤ 5 cm	20(9.7)	11(12.2)		
5 ~ 10 cm	66(31.9)	31(34.4)		
≥ 10 cm	121(58.5)	48(53.3)		
Lesion type/case (%)			1.457[a]	0.483
Parenchymal type	87(42.0)	37(41.1)		
Liquefied type	45(21.7)	25(27.8)		
Mixed type	75(36.3)	28(31.1)		
Calcification signs/case (%)			0.249[a]	0.618
No	32(15.5)	16(17.8)		
Yes	175(84.5)	74(82.2)		
Cavity signs /case (%)			0.614[a]	0.433
No	91(44.0)	44(48.9)		
Yes	116(56.0)	46(51.1)		
PNM stages/case (%)			0.119[a]	0.73
P1, P2	108(52.2)	45(50.0)		
P3, P4	99(47.8)	45(50.0)		
Extent of hepatic involvement/case (%)			0.295[a]	0.587
Limited to half liver	101(48.8)	47(52.2)		
Not limited to half liver	106(51.2)	43(47.8)		
Hepatic gate invasion/case (%)			0.587[a]	0.444
No	105(50.7)	50(55.6)		
Yes	102(49.3)	40(44.4)		
Enhancement status /case (%)			0.544[a]	0.461
No	110(53.1)	52(57.8)		
Yes	97(46.9)	38(42.2)		
Bile duct dilation /case (%)			1.030[a]	0.31
No	128(61.8)	50(55.6)		
Yes	79(38.2)	40(44.4)		
Bile duct invasion/case (%)			0.040[a]	0.842
No	145(70.0)	62(68.9)		
Yes	62(30.0)	28(31.1)		
Hepatic vein invasion/case (%)			0.804[a]	0.37
No	76(36.7)	38(42.2)		
Yes	131(63.3)	53(57.8)		
Inferior vena cava invasion/case (%)			1.099[a]	0.294
No	108(52.2)	41(45.6)		
Yes	99(47.8)	49(54.4)		
Hepatic artery invasion/case (%)			0.034[a]	0.854
No	108(52.2)	48(53.3)		
Continued				

Factors	Training (207)	Test (90)	Statistical values	*p*-values
Yes	99(47.8)	42(46.7)		
Portal vein invasion/case (%)			0.023[a]	0.878
No	58(28.0)	26(28.9)		
Yes	149(72.0)	64(71.1)		
Exposure history to cattle and sheep /case (%)			0.409[a]	0.522
No	35(16.9)	18(20.0)		
Yes	172(83.1)	72(80.0)		
HBV five markers /case (%)			0.065[a]	0.799
Negative	75(36.2)	34(37.8)		
Positive	132(63.8)	56(62.2)		
Treatment methods/case (%)			0.002[a]	0.963
Expectant treatment	119(57.5)	52(57.8)		
Non-conservative treatment	88(42.5)	38(42.2)		
Complications/case (%)			0.656[a]	0.199
No	200(96.6)	86(95.6)		
Yes	7(3.4)	4(4.4)		
Other organ metastases /case (%)			1.135[a]	0.287
No	180(87.0)	74(82.2)		
Yes	27(13.0)	16(17.8)		

Table 1. Comparison of imaging features and clinical indicators between training set and validation set in patients with hepatic alveolar echinococcosis. [a]Indicates the chi-square test; [b]indicates the independent samples T-test. *Indicates that only 52 patients with pulmonary metastasis who underwent MRI examination were selected and compared with 46 randomly selected patients without pulmonary metastasis for analysis.

based on the predictors above demonstrates excellent predictive performance, high agreement between predicted and actual values, and good clinical application value.

There is significant variability in the size of HAE lesions, ranging from sub-millimeter to 3 centimeters[10,24], and this diversity has been observed in multiple studies. A multicenter study[25] has revealed an intriguing phenomenon: compared to the relatively more minor lesions observed in European regions (specifically, with an average size of 70.4 ± 32.3 mm in Besançon and 71.4 ± 46.4 mm in Ulm), the lesions in Xining and Urumqi, China, are notably larger, measuring 108.0 ± 53.0 mm and 132.7 ± 46.0 mm, respectively. Researchers speculate that this difference may be because most Chinese patients reside in remote rural areas with relatively limited economic conditions. Therefore, they often seek medical help only after symptoms appear, usually at a later stage of the disease, allowing the lesions more time to grow and spread. Our study further found that lesion size is an independent predictor of pulmonary metastasis in HAE, which echoes recent research findings by Graeter et al.[6]. They conducted an in-depth study on the evolution of HAE lesions and staged them. They observed that when the lesion volume increases, it usually indicates that the disease has progressed to the "progressive stage" or "advanced stage," during which the lesion activity is significantly enhanced, making it more prone to deterioration and leading to metastasis. This observation has also been further validated in multiple research centers in their studies[20,21]. Meanwhile, Kodama et al.[26] also noted the relationship between lesion size and disease activity in their typing study of HAE lesions. They found that type 2 and type 3 lesions had the most significant volumes, especially type 3 lesions, which exhibited the most significant activity. This finding further supports our research results, which indicate that lesion size is an independent risk factor for HAE metastasis. Collectively, these studies provide us with deeper insights that aid in better understanding and predicting the risk of metastasis in HAE.

The liver is the most common site of involvement in human HAE, accounting for 70% of all cases. It can also disseminate through the bloodstream to various organs throughout the body[2,27,28]. Among them, pulmonary involvement constitutes 20–30% of cases. Less common sites of involvement include the spleen, kidneys, heart, bones, central nervous system, and other organs[10]. Pulmonary alveolar echinococcosis is typically caused by the hematogenous spread of HAE to the pulmonary region, accounting for approximately 0.3% of all cases of systemic echinococcosis. In rare instances, it can arise from direct inhalation of the infectious agent through the respiratory tract or from direct invasion of liver lesions. Graeter et al.[21] conducted an in-depth comparative study of lesions in China and Europe and found that lesions in China are more prone to metastasis. It is speculated that this may be because Chinese cases are often already in the later stages of the disease at the time of diagnosis. These findings reveal the close correlation between distant extrahepatic metastasis and disease progression. Our study further found that patients with metastasis to other organs often have pulmonary metastasis, and it is the strongest independent predictor of pulmonary metastasis. Given the precedence and commonality of pulmonary metastasis in HAE, the author believes that when a patient presents with metastasis to other organs, pulmonary metastasis often already exists. At this point, radical surgical resection becomes no longer feasible, which is currently recognized as the only potentially curative treatment option[29–31]. Therefore, timely prediction

Factors	Training set		Statistical values	*p*-values
	No pulmonary metastasis (136)	Pulmonary metastasis (71)		
Sex/case (%)			0.370[a]	0.543
Male	61(44.9)	35(49.3)		
Famale	75(55.1)	36(50.7)		
Age/Y	36.90 ± 14.11	42.55 ± 12.88	2.817[b]	0.005
Ethnic group/ case (%)			0.001[a]	0.971
Tibet	119(87.5)	62(87.3)		
Other	17(12.5)	9(12.7)		
Marginal zone /case (%)*			0.025[a]	0.875
No	21(45.7)	18(47.4)		
Yes	25(54.3)	20(52.6)		
Microvesicles/case (%)*			3.109[a]	0.078
No	24(52.2)	27(71.1)		
Yes	22(47.8)	11(28.9)		
Number of lesions/case (%)			1.645[a]	0.2
One	98(72.1)	45(63.4)		
Two or more	38(27.9)	26(36.6)		
Lesion size/case (%)			11.861[a]	0.003
≤ 5 cm	15(11.0)	5(7.0)		
5 ~ 10 cm	53(39.0)	13(18.3)		
≥ 10 cm	68(50.0)	53(74.6)		
Lesion type/case (%)			1.300[a]	0.522
Parenchymal type	55(40.4)	32(45.1)		
Liquefied type	28(20.6)	17(23.9)		
Mixed type	53(39.0)	22(31.0)		
Calcification signs/case (%)			2.593[a]	0.107
No	25(18.4)	7(9.9)		
Yes	111(81.6)	64(90.1)		
Cavity signs /case (%)			12.091[a]	0.001
No	48(35.3)	43(60.6)		
Yes	88(64.7)	28(39.4)		
PNM stages/case (%)			2.185[a]	0.139
P1, P2	76(55.9)	32(45.1)		
P3, P4	60(44.1)	39(54.9)		
Extent of hepatic involvement/case (%)			5.011[a]	0.025
Limited to half liver	74(54.4)	27(38.0)		
Not limited to half liver	62(45.6)	44(62.0)		
Hepatic gate invasion/case (%)			14.527[a]	< 0.001
No	82(60.3)	23(32.4)		
Yes	54(39.7)	48(67.6)		
Enhancement status /case (%)			9.081[a]	0.003
No	62(45.6)	48(67.6)		
Yes	74(54.4)	23(32.4)		
Bile duct dilation /case (%)			12.871[a]	< 0.001
No	96(70.6)	32(45.1)		
Yes	40(29.4)	39(54.9)		
Bile duct invasion/case (%)			2.290[a]	0.13
No	100(73.5)	45(63.4)		
Yes	36(26.5)	26(36.6)		
Hepatic vein invasion/case (%)			0.000[a]	0.984
No	50(36.8)	26(36.6)		
Yes	86(63.2)	45(63.4)		
Inferior vena cava invasion/case (%)			0.000[a]	0.99
No	71(52.2)	37(52.1)		
Yes	65(47.8)	34(47.9)		
Hepatic artery invasion/case (%)			1.405[a]	0.236
Continued				

Factors	Training set		Statistical values	*p*-values
	No pulmonary metastasis (136)	Pulmonary metastasis (71)		
No	75(55.1)	33(46.5)		
Yes	61(44.9)	38(53.5)		
Portal vein invasion/case (%)			0.085[a]	0.771
No	39(28.7)	19(26.8)		
Yes	97(71.3)	52(73.2)		
Exposure history to cattle and sheep /case (%)			9.754[a]	0.002
No	15(11.0)	20(28.2)		
Yes	121(89.0)	51(71.8)		
HBV five markers /case (%)			0.151[a]	0.698
Negative	48(35.3)	27(38.0)		
Positive	88(64.7)	44(62.0)		
Treatment methods/case (%)			13.021[a]	< 0.001
Expectant treatment	66(48.5)	53(74.6)		
Non-conservative treatment	70(51.5)	18(25.4)		
Complications/case (%)			3.782[a]	0.052
No	129(94.9)	71(100.0)		
Yes	7(5.1)	0(0.0)		
Other organ metastases /case (%)			21.798[a]	< 0.001
No	129(94.9)	51(71.8)		
Yes	7(5.1)	20(28.2)		

Table 2. Univariate analysis of the association between imaging features, clinical indicators, and pulmonary metastasis in patients with hepatic alveolar echinococcosis in the training set. [a]Indicates the chi-square test; [b]indicates the independent samples T-test. *Indicates that within the training set, only 38 patients with pulmonary metastasis who underwent MRI examination were selected, and 46 patients without pulmonary metastasis were randomly selected for comparative analysis.

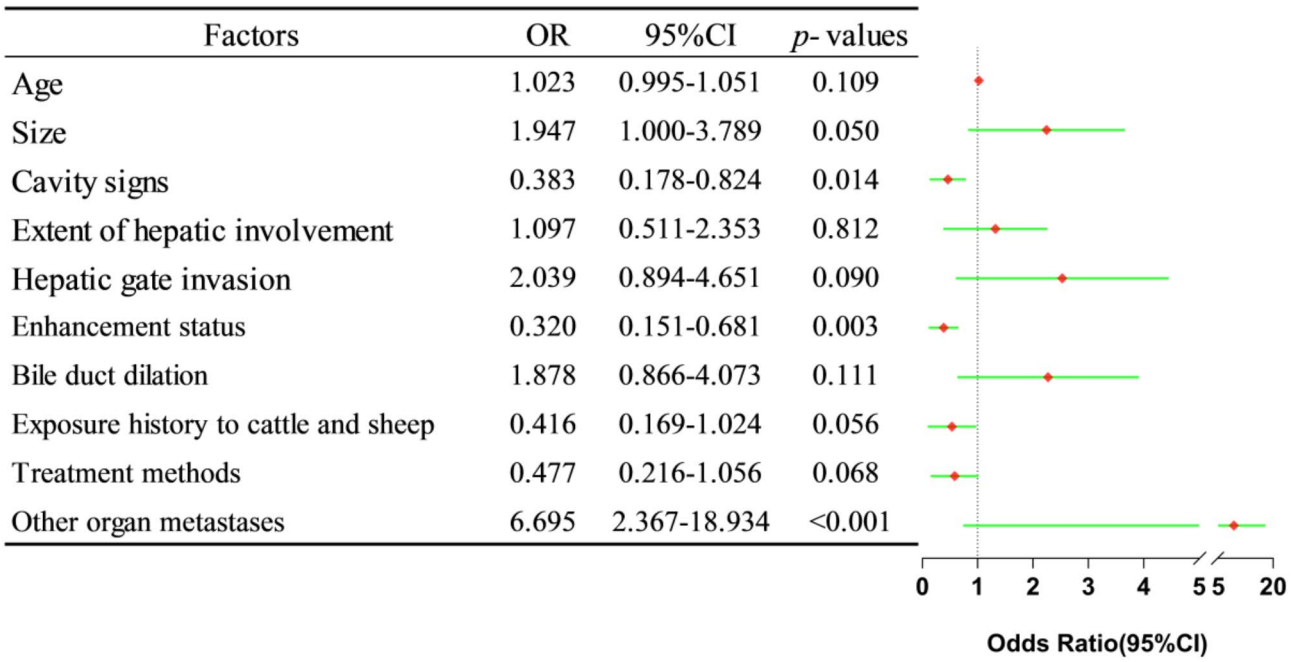

Fig. 4. Multivariate analysis of the association between imaging features, clinical indicators, and lung metastasis in patients with hepatic alveolar echinococcosis from the training set, along with the corresponding forest plot.

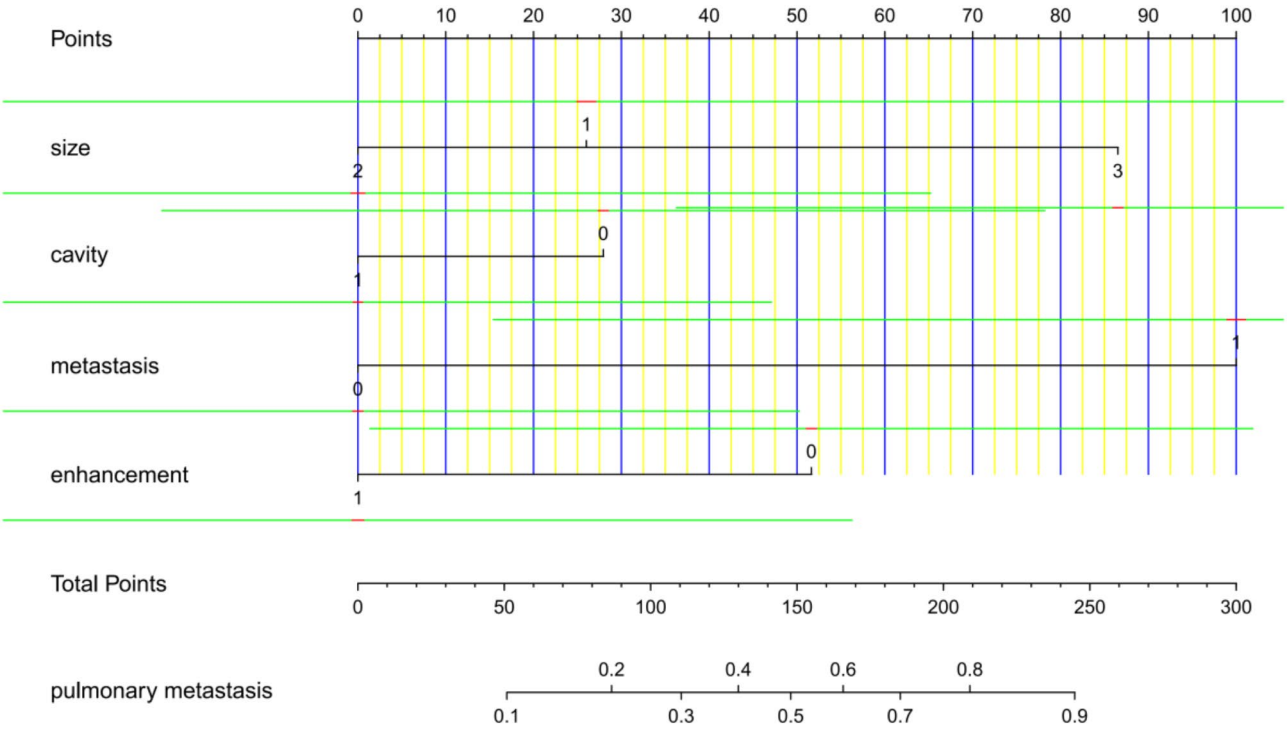

Fig. 5. Nomogram of the prediction model for pulmonary metastasis in patients with hepatic alveolar echinococcosis, where the green line represents the 95% confidence interval.

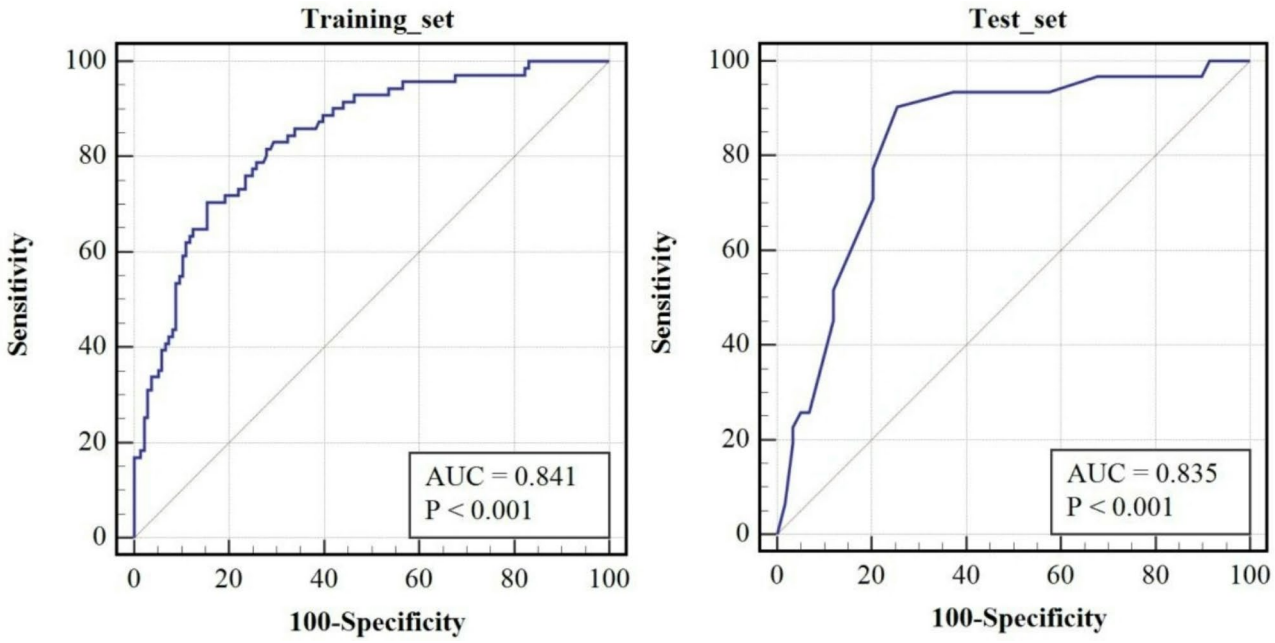

Fig. 6. (**A**) ROC curve for the training set; (**B**): ROC curve for the test set.

of pulmonary metastasis not only helps to prevent further deterioration of the disease but also provides a solid basis for selecting the optimal treatment for patients, significantly improving their prognosis.

Notably, our study not only uncovered the critical role of lesion size and other organ metastases in promoting pulmonary metastasis but also identified the cavity signs of the lesion and its enhancement as hindering factors for pulmonary metastasis. This discovery provides a new perspective for us to understand the complex mechanism of pulmonary metastasis more comprehensively.

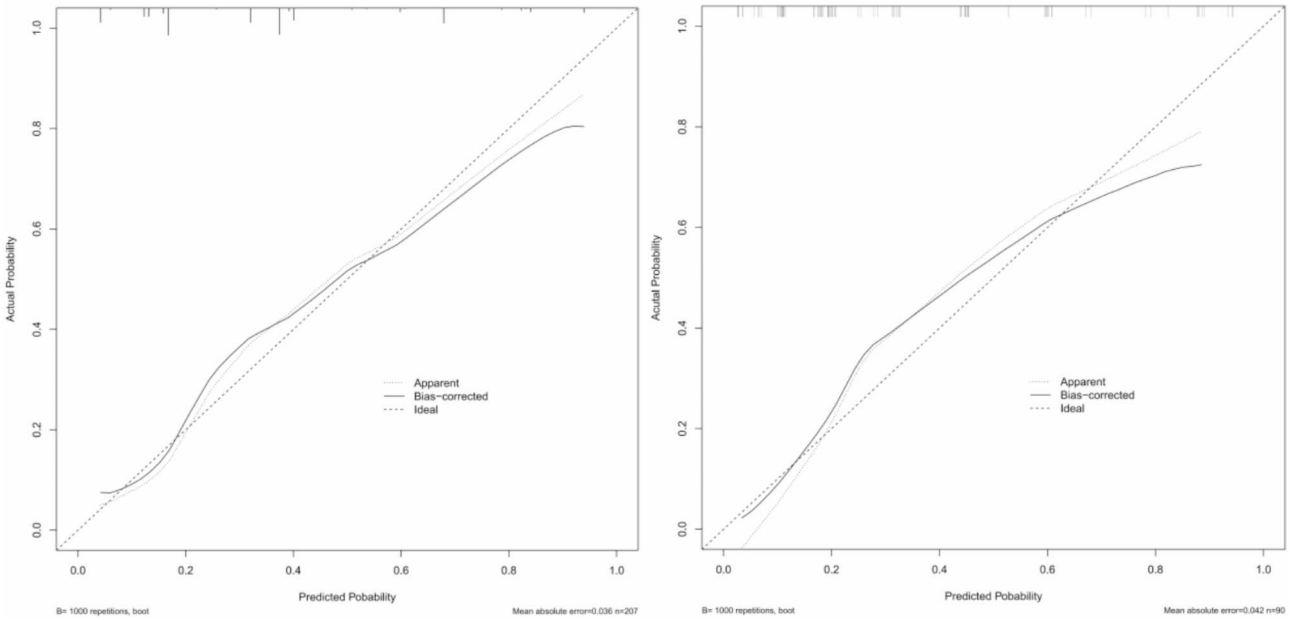

Fig. 7. (**A**) Calibration curve for the training set with a mean absolute error of 0.036; (**B**) Calibration curve for the validation set with a mean absolute error of 0.042.

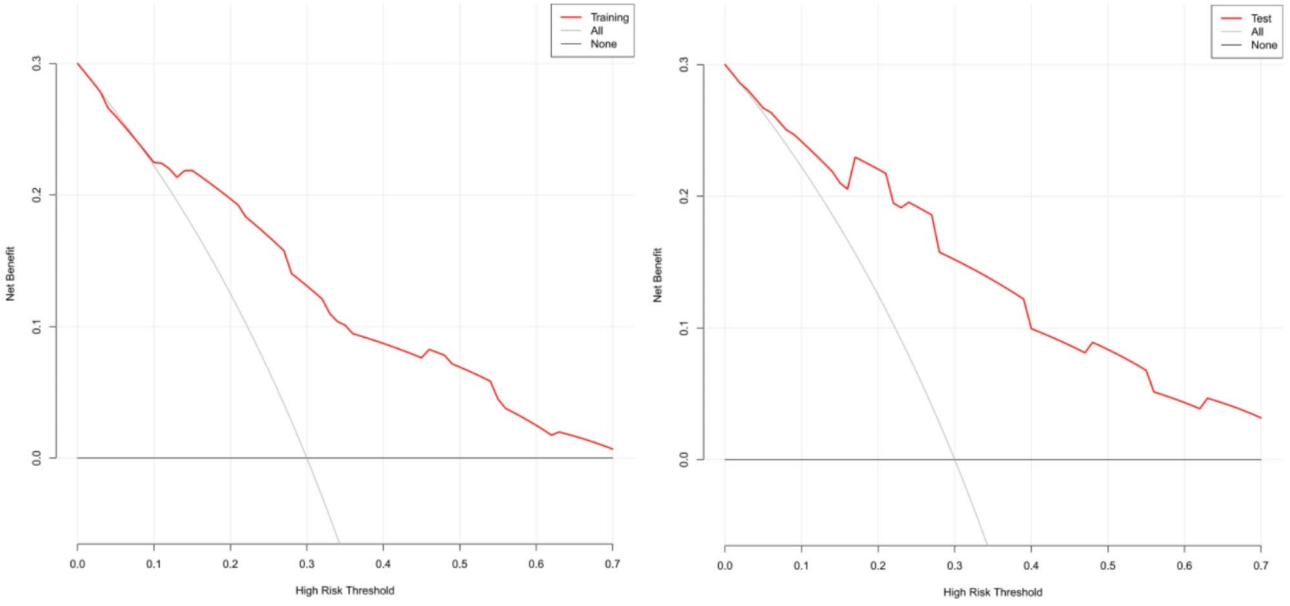

Fig. 8. (**A**) Decision Curve Analysis curve for the training set; (**B**) Decision curve analysis curve for the validation set.

HAE spreads indefinitely outward and invades surrounding tissues through exogenous budding proliferation[3], continuously generating new vesicles that grow into the tissue. The study by Graeter et al.[6] revealed that the evolution of HAE typically goes through five stages: "an initial stage, progressive stage, advanced stage, transitional stage, and regressive stage." During the transitional stage, degenerative changes gradually occur in the center of the lesion, with internal coagulation and vascular occlusion leading to localized ischemic necrosis and the appearance of cavity signs. At this point, the lesion has significantly decreased, and the possibility of reactivation and exacerbation has also notably decreased. In the "transitional stage" AE cases we observed, the cavity signs are often a product of necrotic lesions containing multiple degenerative microcysts and associated immune infiltration and fibrosis. In their study of extrahepatic metastasis, Graeter et al.[21] discovered that the primary morphological types IV and V of liver lesions were not linked to any cases of distant extrahepatic metastasis. On the contrary, varying degrees of distant extrahepatic metastasis were observed in types I-III, with

type III being the most prominent, accounting for 22% of cases. Our study also found that patients exhibiting cavity signs are less prone to pulmonary metastasis, indicating that these lesions gradually progress towards the regressive stage and their activity has decreased considerably. This discovery coincides with the findings from the research above, providing us with a method to roughly judge the progression of lesions by observing specific imaging signs. Thus, we can promptly take effective treatment measures to reduce lesion activity, avoid the occurrence of pulmonary metastasis, and improve patients' prognosis.

HAE is mainly manifested as irregular, mixed density/signal solid or cystic masses in the liver on imaging[19], with no significant enhancement after contrast administration. Mild enhancement can be seen around some lesions, and there is currently debate about the specific composition of this area. Some scholars believe it is an active proliferative region of HAE[29], while others consider it an inflammatory reaction zone[32]. Our postoperative pathological analysis showed that most cases were dominated by inflammatory granulation tissue, with only a few showing scoleces. Therefore, we believe that the surrounding enhanced area is mainly composed of inflammatory components, with only a tiny portion being the active area of HAE. Studies have shown that the granulation tissue at the edge of HAE lesions is rich in various functional types of macrophages[33], including typical epithelioid cells, giant cells, and different types of T lymphocytes[34], among which the Th1-type immune response of helper T cells has the potential to prevent larval proliferation. Wang et al.[35] believe that the surrounding strong fibrous inflammatory response partially restricts the proliferative capacity of parasite tissue. They also suggest that dendritic cells (DCs) and macrophages (MØs) are among the first cells to come into contact with parasites, and these cells can manage immune orientation, effectively controlling and inhibiting parasite proliferation. The study by Liu et al.[36] also confirmed that the prolonged inflammatory response caused by HAE infection triggers the self-protection and repair mechanism of the liver microenvironment, leading to massive proliferation and renewal of KCs and promoting the release of anti-inflammatory cytokines by M2-like macrophages to resist the stimulation of AHE. In this study, we observed that the enhancement surrounding the lesion impeded pulmonary metastasis. Based on the above studies, we speculate that various functional types of macrophages in the inflammatory region around HAE lesions are essential in hindering pulmonary metastasis. These findings provide a new perspective for us to understand the pathogenesis of HAE deeply and also offer potential targets for future treatment strategies.

Nomograms are visual tools used to optimize statistical models[37]. By skillfully integrating various predictors and outcome variables, they provide us with an intuitive method for predicting event probabilities, thereby meeting individualized healthcare needs. It has demonstrated broad application value in clinical practice[38,39]. This study delved into some relevant clinical and imaging information regarding pulmonary metastasis in HAE patients and successfully identified independent predictors of pulmonary metastasis, including lesion size, other organ metastases, cavity signs, and enhancement. Based on these independent influencing factors, a prediction model for pulmonary metastasis was constructed and vividly presented as a nomogram. After rigorous training on the training set and testing on the test set, the model has demonstrated excellent predictive performance. The calibration curve further verifies the high agreement between the predicted values of the nomogram and the actual values. Meanwhile, decision curve analysis also fully demonstrates the great value of this nomogram in clinical practice. It can provide doctors with a noninvasive, quantitative, and convenient way to quickly identify potential risk factors for pulmonary metastasis and then develop personalized treatment plans for patients to maximize their benefits.

However, this study has some limitations: Firstly, it is a retrospective study, which may have some selection bias. Secondly, the single-center nature of this study limits the broad application of the model. Further multi-center studies are needed to validate its predictive performance and improve the model's generality and adaptability. Finally, limited by the sample size, the applicability of the results of this study in larger populations still needs to be further validated. Therefore, we look forward to conducting more clinical studies on a larger scale to improve and continuously validate this research's findings.

Conclusion

In summary, this study successfully constructed a nomogram prediction model for pulmonary metastasis of HAE based on lesion size, other organ metastases, cavity signs, and enhancement. It achieved early, accurate, objective, noninvasive, and intuitive prediction of the risk of pulmonary metastasis in HAE patients, providing clinicians with a deeper understanding of disease progression and a solid basis for selecting individualized treatment plans for patients, thereby ensuring optimal prognostic outcomes.

Data availability

The datasets used and analyzed during the current study are available from the corresponding author on reasonable request.

Received: 13 November 2024; Accepted: 2 April 2025
Published online: 14 May 2025

References

1. Vuitton, D. A. et al. International consensus on terminology to be used in the field of echinococcoses. *Parasite* **27**, 41 (2020).
2. Guo, H., Liu, W., Wang, J. & Xing, Y. Extrahepatic alveolar Echinococcus on multi-slice computed tomography and magnetic resonance imaging. *Sci. Rep.* **11**, 9409 (2021).
3. Kantarci, M., Aydin, S., Eren, S., Ogul, H. & Akhan, O. Imaging aspects of hepatic alveolar echinococcosis: retrospective findings of a surgical center in Turkey. *Pathogens* **11**, 276 (2022).
4. Romig, T. et al. Ecology and life cycle patterns of *Echinococcus* species. *Adv. Parasitol.* **95**, 213–314 (2017).
5. Kern, P. et al. The echinococcoses: Diagnosis, clinical management and burden of disease. *Adv. Parasitol.* **96**, 259–369 (2017).

6. Graeter, T., Schmidberger, J. & Stage-Oriented, C. T. Classification and intermodal evolution model in hepatic alveolar echinococcosis. *Rofo* **194**, 532–544 (2022).
7. Kern, P. et al. European echinococcosis registry: Human alveolar echinococcosis, Europe, 1982–2000. *Emerg. Infect. Dis.* **9**, 343–349 (2003).
8. Calame, P. et al. Local invasion of hepatic alveolar echinococcosis should not be underestimated: Lessons learned from imaging-pathologic correlation. *Diagn. Interv Imaging* **102**, 189–192 (2021).
9. Baumann, S. et al. Worldwide literature on epidemiology of human alveolar echinococcosis: A systematic review of research published in the twenty-first century. *Infection* **47**, 703–727 (2019).
10. Xin, S. et al. Automatic lesion segmentation and classification of hepatic echinococcosis using a multiscale-feature convolutional neural network. *Med. Biol. Eng. Comput.* **58**, 659–668 (2020).
11. Brunetti, E., Kern, P. & Vuitton, D. A. Expert consensus for the diagnosis and treatment of cystic and alveolar echinococcosis in humans. *Acta Trop.* **114**, 1–16 (2010).
12. Ren, B. et al. Hepatic alveolar echinococcosis: predictive biological activity based on radiomics of MRI. *Biomed. Res. Int.* **2021** (6681092). https://doi.org/10.1155/2021/6681092 (2021).
13. Tian, P. et al. The value of nomogram analysis in prediction of cerebral spread of hepatic alveolar echinococcosis. *Acta Trop.* **260**, 107429. https://doi.org/10.1016/j.actatropica.2024.107429 (2024).
14. Zhou, Y. et al. A CT-based radiomics model for predicting lymph node metastasis in hepatic alveolar echinococcosis patients to support lymph node dissection. *Eur. J. Med. Res.* **29**, 409. https://doi.org/10.1186/s40001-024-01999-x (2024).
15. Zhang, S. et al. Value of intralesional and perilesional radiomics for predicting the bioactivity of hepatic alveolar echinococcosis. *Front. Oncol.* **14**, 1389177. https://doi.org/10.3389/fonc.2024.1389177 (2024).
16. Lin, X., Shao, Y. M., Zhang, R. Q. & Aji, T. Applying LASSO logistic regression for the prediction of biliary complications after ex vivo liver resection and autotransplantation in patients with end-stage hepatic alveolar echinococcosis. *Eur. J. Med. Res.* **29**, 301. https://doi.org/10.1186/s40001-024-01898-1 (2024).
17. The Chinese Society of Radiology Infectious Disease Imaging Group, the Chinese Medical Doctor Association Radiology Physician Branch Infection Imaging Special Committee. Expert consensus on imaging diagnosis of hepatic echinococcosis. *Chin. J. Radiol.*, **55**, 5–11 .
18. Eroglu, A., Ogul, H. & Aydin, Y. CT imaging findings of pulmonary alveolar echinococcosis. *Curr. Med. Imaging* **19**, 97–102 (2023).
19. Yu, X. K., Zhang, L., Ma, W. J., Bi, W. Z. & Ju, S. G. An overview of hepatic echinococcosis and the characteristic CT and MRI imaging manifestations. *Infect. Drug Resist.* **14**, 4447–4455 (2021).
20. Graeter, T. et al. Intrahepatic manifestation and distant extrahepatic disease in alveolar echinococcosis: A multicenter cohort study. *Acta Radiol.* **62**, 997–1005 (2021).
21. Graeter, T. et al. Evaluation of intrahepatic manifestation and distant extrahepatic disease in alveolar echinococcosis. *World J. Gastroenterol.* **26**, 4302–4315 (2020).
22. Brumpt, E. et al. AE hepatic lesions: Correlation between calcifications at CT and FDG-PET/CT metabolic activity. *Infection* **47**, 955–960 (2019).
23. Wen, H. et al. Echinococcosis: Advances in the 21st century. *Clin. Microbiol. Rev.* **32**, e00075–e00018 (2019).
24. Dietrich, C. F. et al. Cystic and alveolar echinococcosis of the hepatobiliary tract - the role of new imaging techniques for improved diagnosis. *Med. Ultrason.* **22**, 75–84 (2020).
25. Graeter, T. et al. Hepatic alveolar echinococcosis: Comparative computed tomography study between two Chinese and two European centres. *Food Waterborne Parasitol.* **19**, e00082 (2020).
26. Kodama, Y. et al. Alveolar echinococcosis: MR findings in the liver. *Radiology* **228**, 172–177 (2003).
27. Stefaniak, M., Derda, M., Zmora, P. & Nowak, S. P. Risk factors and the character of clinical course of the *Echinococcus multilocularis* infection in patients in Poland. *Pathogens* **12**, 199 (2023).
28. Gottstein, B. & Deplazes, P. Alveolar echinococcosis: What triggers emergence in North America, central Europe and Asia. *Curr. Opin. Infect. Dis.* **34**, 440–446 (2021).
29. Calame, P. et al. Role of the radiologist in the diagnosis and management of the two forms of hepatic echinococcosis. *Insights Imaging* **13**, 68 (2022).
30. Sulyok, M. et al. Implementing deep learning models for the classification of Echinococcus multilocularis infection in human liver tissue. *Parasit. Vectors* **16**, 29 (2023).
31. Brumpt, É. et al. Kodama-XUUB: an informative classification for alveolar echinococcosis hepatic lesions on magnetic resonance imaging. *Parasite* **28**, 66 (2021).
32. Bulakçı, M. et al. Multimodality imaging in diagnosis and management of alveolar echinococcosis: An update. *Diagn. Interv Radiol.* **22**, 247–256 (2016).
33. Vuitton, D. A. & Gottstein, B. Echinococcus multilocularis and its intermediate host: a model of parasite-host interplay. *J. Biomed. Biotechnol.* 923193. (2010).
34. Bresson-Hadni, S. et al. Cellular immunity in experimental *Echinococcus multilocularis* infection. II. Sequential and comparative phenotypic study of the periparasitic mononuclear cells in resistant and sensitive mice. *Clin. Exp. Immunol.* **82**, 378–383 (1990).
35. Wang, J. & Gottstein, B. Immunoregulation in larval *Echinococcus multilocularis* infection. *Parasite Immunol.* **38**, 182–192 (2016).
36. Liu, Y. et al. Kupffer cells: important participant of hepatic alveolar echinococcosis. *Front. Cell. Infect. Microbiol.* **10**, 8 (2020).
37. Wang, T. et al. A competing risk model nomogram to predict the Long-Term prognosis of lung carcinoid. *Ann. Surg. Oncol.* **30**, 5830–5839 (2023).
38. Chen, Y. D. et al. Radiomics and nomogram of magnetic resonance imaging for preoperative prediction of microvascular invasion in small hepatocellular carcinoma. *World J. Gastroenterol.* **28**, 4399–4416 (2022).
39. Yue, X. et al. Multiparametric magnetic resonance imaging-based radiomics nomogram for predicting tumor grade in endometrial cancer. *Front. Oncol.* **13**, 1081134 (2023).

Acknowledgements

We sincerely thank the Affiliated Hospital of Qinghai University for providing the data for the training set and external validation set.

Author contributions

H.B. conceptualized the study and provided guidance for this work. C.L. designed the methodology, performed model validation and statistical analyses. C.L. and Y.D. prepared the original draft. All authors contributed to the review and editing of the manuscript. Haihua Bao was responsible for the acquisition of the financial support for the project leading to this publication. C.L. and Y. D. contributed equally to this article.

Funding

Open access funding provided by National Key Specialty Program.

Declarations

Competing interests
The authors declare no competing interests.

Ethical approval
The research protocol for this study was approved by the Ethics Committee of the Clinical Medical College of Qinghai University, under approval number P-SL-2023-229. Given that this study is retrospective in nature, the Ethics Committee granted a waiver for informed consent. All research procedures were conducted in accordance with relevant ethical guidelines and regulations.

Additional information
Correspondence and requests for materials should be addressed to H.B.

Reprints and permissions information is available at www.nature.com/reprints.

Publisher's note Springer Nature remains neutral with regard to jurisdictional claims in published maps and institutional affiliations.